Role of Interference between Localized and Propagating Surface Waves on the Extraordinary Optical Transmission Through a Subwavelength-Aperture Array

Yong-Jun Bao,[1] Ru-Wen Peng,[1,*] Da-Jun Shu,[1] Mu Wang,[1,*] Xiang Lu,[2] Jun Shao,[2] Wei Lu,[2] and Nai-Ben Ming[1]

[1]*National Laboratory of Solid State Microstructures & Department of Physics, Nanjing University, Nanjing 210093, China*

[2]*National Laboratory for Infrared Physics, Shanghai Institute of Technical Physics, Chinese Academy of Sciences, Shanghai 200083, China*

(Received 14 January 2008; revised manuscript received 13 July 2008; published 20 August 2008)

We report in this Letter that when radiation is incident on a metal surface perforated with an array of ring-shaped subwavelength apertures, the phase difference between the propagating surface Bloch wave and the localized surface wave can be tailored by the geometrical parameters of the array so as to affect the shape of the transmission spectrum. Above the resonant frequency of the aperture, interference between the two kinds of surface waves leads to a minimum in the transmission spectrum, whereas below it, the interference leads to a maximum. We suggest that this feature provides flexibility in engineering surface-wave-based all-optical devices.

DOI: 10.1103/PhysRevLett.101.087401 PACS numbers: 78.67.−n, 42.25.−p, 78.66.Bz, 78.68.+m

The extraordinary optical transmission through arrays of subwavelength apertures on metal films has recently attracted much attention [1–13]. This phenomenon was initially suggested to be associated with surface plasmon polariton (SPP). With the help of the reciprocal lattice vectors provided by periodic arrays of subwavelength apertures (ASWA) on a metal surface, a surface Bloch wave can be excited by the incident light [1–9]. More recently, it was also proposed that due to the dynamic diffraction of the incident wave by interfacial microstructures, composite diffracted evanescent waves are generated and contribute to the extraordinary light transmission [10]. Now the physical processes governing the extraordinary transmission can be understood as follows. The excited surface electromagnetic Bloch wave on the structured metal surface enhances the evanescent field at the apertures and thus contributes to funneling light through the aperture array [12,13]. We denote this transmitted field of the propagating surface modes (PSM) as $\boldsymbol{E}_{\mathrm{PSM}}$. In addition to the propagating surface wave, there also exists a regional resonant excitation around each aperture, which is known as the localized surface mode (LSM) [14–18]. The incident light may partially transmit through the subwavelength apertures on metal film, bearing the phase configuration contributed by LSM around the aperture [14]. We denote this portion of light as $\boldsymbol{E}_{\mathrm{LSM}}$. Although the interaction of interfacial waves on metallic surfaces has been investigated before [10,19–24], previous studies have focused either on the interference of incident wave with PSM [10,19,20], or on the coupling of surface waves associated with SPP [14,17,21–24]. The detailed coupling process of these waves, however, has not been directly addressed.

We report here that the transmission spectrum can be tuned by the geometrical parameters of an array of subwavelength ring-shaped apertures, which can be ascribed to the change of phase difference between the excited propagating surface wave $\boldsymbol{E}_{\mathrm{PSM}}$ and the localized surface wave $\boldsymbol{E}_{\mathrm{LSM}}$. Above the resonant frequency for the ring-shaped aperture, destructive interference between the two kinds of surface waves leads to a minimum in the transmission spectrum, whereas below the resonant frequency, constructive interference leads to a maximum.

Two types of aperture arrays are prepared on gold films by photolithography [25]. The first type consists of open square apertures. The edge of each square aperture is 2.0 μm, and the lattice parameter is 6.0 μm [Fig. 1(a)]. The second type is a square aperture centered with a compact square metallic patch, forming a ring-shaped evacuated region. The outer edge of the aperture is 2.0 μm long, the central patch is 1.0 μm [Fig. 1(b)], and the lattice parameter is the same as that of Fig. 1(a). The transmission spectrum of an individual aperture of each type is calculated by finite-difference time-domain (FDTD) method [26]. For the open square aperture, in the midinfrared frequency range, the transmission increases monotonically as the wave number increases [Fig. 1(c)]. For the ring-shaped aperture, a distinct resonant peak appears at $\nu_0 = 968.75\ \mathrm{cm}^{-1}$ [Fig. 1(d)]. The phase shift of light transmitted through an individual aperture on a metallic film with respect to that propagating in free space, $\varphi(\nu)$, is calculated. For an isolated open square aperture, $\varphi(\nu)$ varies from 0.468π to 0.012π [Fig. 1(e)]. For an isolated ring-shaped aperture, $\varphi(\nu)$ varies from 0.461π to -0.264π, and zero phase shift occurs near the resonance frequency ν_0 [Fig. 1(f)]. The resonance behavior of an aperture is analogous to an inductive-capacitive circuit [27], where $\varphi(\nu)$ varies in the range of $[\pi/2, 0]$ for an open aperture, and in $[-\pi/2, \pi/2]$ for a ring-shaped aperture [28].

The transmission spectra of the aperture array on gold film are shown in Fig. 2. The FDTD calculation for an open aperture array is illustrated by the solid line in Fig. 2(a). Four distinct peaks are located at 476.56 cm^{-1}, 667.97 cm^{-1}, 953.13 cm^{-1}, and 1058.59 cm^{-1}, respec-

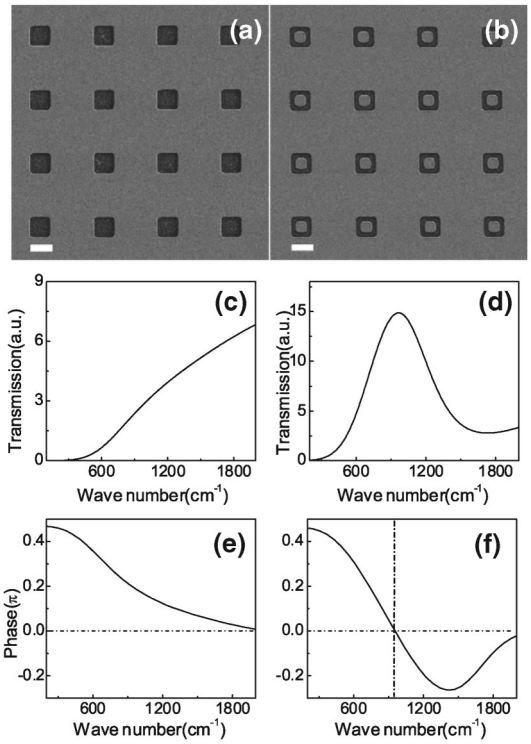

FIG. 1. SEM micrographs of arrays of open square apertures (a) and ring-shaped apertures with a central solid square metal patch (b). The bar represents 2.0 μm. (c) and (d) are the FDTD calculated spectra of an open aperture and a ring-shaped aperture, respectively. (e) and (f) show the phase shifts of an electromagnetic wave passing through an individual open square aperture and a ring-shaped aperture with respect to the free propagation wave, respectively.

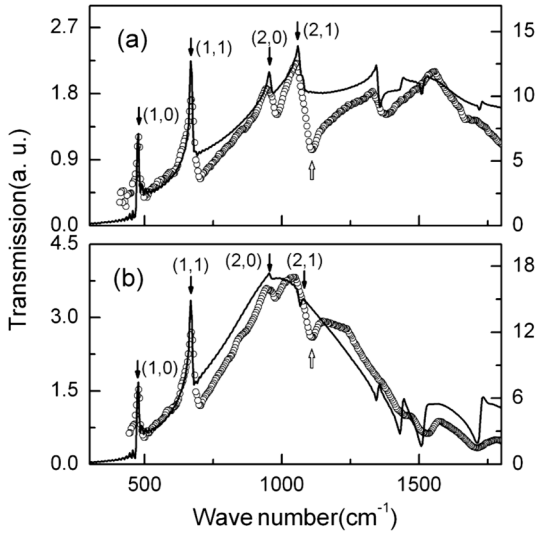

FIG. 2. The transmission spectra of arrays of open square apertures (a) and ring-shaped apertures (b). The solid lines are the calculated spectra and the open circles are the experimental data. The scale on the left side of the figure is for experimental data, and that on the right side is for the calculated spectra (the same in Figs. 3 and 4).

tively. The open circles are the experimental data, which are in agreement with the calculation. The solid line in Fig. 2(b) is the calculated result for the ring-shaped aperture array. Three peaks are located at 476.56 cm^{-1}, 667.97 cm^{-1}, and 953.13 cm^{-1}, respectively, and a dip appears at 1058.59 cm^{-1}. The wide bump around $\nu_0 =$ 968.75 cm^{-1} is due to the resonance of LSM. The experimental data are in good agreement with the calculation, except near 1108.9 cm^{-1} (as indicated by the open arrow), where the absorption of the silicon substrate [29] obscures the detailed features that appear in the calculation. Figure 2 (b) shows that below the resonance frequency of the aperture (ν_0), enhanced transmission (peak) appears at the specific frequencies, whereas above ν_0, suppressed transmission (dip) occurs instead. By changing either the aperture configuration or the lattice parameter of the array, both the position of transmission extrema and the value of ν_0 can be tuned.

As normal incident light interacts with the periodic aperture array at the air-metal interface, extraordinary transmission occurs at $\nu_{\text{ext}} = \frac{c}{n_{\text{eff}}} G_{i,j}$ [1], where n_{eff} is the effective refractive index of the perforated metallic film, c is the vacuum light velocity (for convenience, c is taken as unity), $G_{i,j} = (\sqrt{i^2 + j^2})/P$ is the reciprocal lattice vector of ASWA, P is the spatial period of the array, and i and j are integers. Accordingly, the extrema located at 476.56 cm^{-1}, 667.97 cm^{-1}, 953.13 cm^{-1}, and 1058.59 cm^{-1}, as shown in Fig. 2(a), are indexed as (1, 0), (1, 1), (2, 0), and (2, 1), which correspond to the reciprocal lattice vectors $G_{1,0}$, $G_{1,1}$, $G_{2,0}$, and $G_{2,1}$ of the array, respectively. Note that for an open square aperture, there is no resonance peak in the midinfrared frequency range [Fig. 1(c)]. Therefore, four peaks emerge, as shown in Fig. 2(a). For the ring-shaped aperture in Fig. 1(b), the resonant peak appears at $\nu_0 = 968.75$ cm^{-1}. Therefore, the modes indexed as (1, 0), (1, 1), (2, 0) are enhanced, whereas mode (2, 1) is suppressed [Fig. 2(b)].

We suggest that the detailed features of the extrema in the transmission spectrum are determined by the difference between the interference amplitude of $\boldsymbol{E}_{\text{PSM}}$ and $\boldsymbol{E}_{\text{LSM}}$ and the amplitude of $\boldsymbol{E}_{\text{LSM}}$ only. For a given ASWA, at the frequency corresponding to G_{ij}, the interference of $\boldsymbol{E}_{\text{PSM}}$ and $\boldsymbol{E}_{\text{LSM}}$ gives

$$E_{\text{out}}(\nu) = E_{\text{LSM}} + E_{\text{PSM}} = \alpha(\nu) e^{i\varphi(\nu)} E_{\text{in}}(\nu) + \beta e^{i\theta_{\text{int}}} E_{\text{in}}(\nu), \quad (1)$$

where $E_{\text{in}}(\upsilon)$ is the electric field of the incident light. Since interference occurs only at frequencies corresponding to G_{ij}, the amplitude and the phase shift of PSM, β and θ_{int}, are taken as constants. Yet the amplitude and phase shift of LSM, $\alpha(\nu)$, and $\varphi(\nu)$ are frequency dependent [28]. It follows that the difference between the interference intensity and the background, ζ, can be written as

$$\zeta = E_{\text{out}}(\nu)E_{\text{out}}(\nu)^* - E_{\text{LSM}}E_{\text{LSM}}^* = \beta^2 + 2\alpha\beta\cos[\varphi(\nu) - \theta_{\text{int}}]. \quad (2)$$

If ζ is positive, a peak appears in the transmission spectrum; if ζ is negative, a dip appears instead. Since the cosine term in Eq. (2) has a range of $[-1, 1]$, ζ is always positive when $\alpha < \beta/2$ and dips do not appear in the transmission spectrum. When α is comparable to β, whether the extremum is a peak or a dip in the spectrum depends on the phase shift between $\boldsymbol{E}_{\text{LSM}}$ and $\boldsymbol{E}_{\text{PSM}}$, $\varphi(\nu) - \theta_{\text{int}}$.

We have numerically calculated $\varphi(\nu)$ for the different types of apertures [Figs. 1(e) and 1(f)]. The value of θ_{int} can be estimated from the behavior of extrema in the transmission spectrum accordingly. Bearing in mind that for the structure shown in Fig. 1(b), the interaction of the surface waves is constructive below ν_0 ($\zeta > 0$) and is destructive above ν_0($\zeta < 0$), and the transition occurs at ν_0 with $\zeta(\nu_0) = 0$; one may get θ_{int} from Eq. (2). Meanwhile, we apply $\varphi(\nu_0) = 0$ based on Fig. 1(f). It follows that θ_{int} equals to $\arccos(-\frac{\beta}{2\alpha})$ for the ring aperture, which is within $[\pi/2, \pi]$. If we suppose that the amplitude of $\boldsymbol{E}_{\text{PSM}}$ equals to that of $\boldsymbol{E}_{\text{LSM}}$, we get $\theta_{\text{int}} = \frac{2}{3}\pi$.

By changing the configuration of the aperture array, the extremum in the transmission spectrum can be tuned from a peak to a dip, and *vice versa*. For example, consider preserving the shape of each individual aperture while increasing the lattice parameter of the array. The resonant frequency of each individual aperture, ν_0, is unchanged, whereas the frequency of the resonant excitation indexed as (i, j) decreases. Once a dip indexed as (i, j) shifts to the left of ν_0, it changes to a peak, meaning that a previously destructive interference becomes a constructive one. If, however, we keep the shape of each individual aperture and decrease the lattice parameter, the extrema move to higher frequencies. In this way, more dips appear.

Instead of changing lattice parameter, the transmission spectra can also be tuned by changing the aperture configuration. For example, if the size of each central square patch of ring-shaped aperture shrinks, ν_0 increases. Consequently, some dips in previous transmission spectrum become peaks.

To verify the above analysis, we have fabricated arrays of ring-shaped apertures with different structural parameters. In the first series of samples, the size of the central patch is fixed at 1.0 μm, and the lattice parameter for the array changes from 4.0 μm to 8.0 μm. For the second series of samples, the lattice parameter is kept at 3.0 μm, and the size of the central patch changes from 0.6 μm to 1.0 μm. In the first series, the aperture shape is fixed, so the resonant feature of LSM is kept, whereas the surface diffraction of the PSMs is tuned when the lattice parameter of the array is changed. Meanwhile, the calculated and the measured transmission spectra are shown in Fig. 3. We focus on four resonant modes indexed as (1,0), (1,1), (2,0), and (2,1). For the array with lattice parameter 8.0 μm, the resonant modes (1, 0), (1, 1), (2, 0), and (2,1) appear at 358.59 cm^{-1}, 503.13 cm^{-1}, 713.28 cm^{-1}, and 791.41 cm^{-1}, respectively, all below the resonant frequency of the individual aperture ν_0 (968.75 cm^{-1}). Consequently, four distinct peaks are generated [Fig. 3(a)]. When the lattice parameter of the array is decreased to 6.0 μm, resonant modes (1, 0), (1, 1), and (2, 0) appear at 476.56 cm^{-1}, 667.97 cm^{-1}, and 953.13 cm^{-1}, which are all below ν_0. The mode (2, 1) appears at 1066.41 cm^{-1}, which is above ν_0. Consequently, mode (2, 1) tunes to a dip while the others are peaks, as shown in Fig. 3(b). When the lattice parameter is further decreased to 4.0 μm, the modes (1, 1), (2, 0), and (2, 1) appear at 1017.97 cm^{-1}, 1432.03 cm^{-1}, and 1592.19 cm^{-1}, respectively, which are all higher than ν_0. So, three dips occur [Fig. 3(c)]. The experimental data are consistent with the calculations.

For the second series, LSM resonance is tuned by changing the shape of each aperture, whereas the surface diffraction process is fixed since the lattice parameter of the array remains the same. Meanwhile, the transmission spectra are shown in Fig. 4. The calculated resonant frequency ν_0 of each individual aperture with patch size 0.6 μm, 0.8 μm, and 1.0 μm appears at 1684.57 cm^{-1}, 1240.63 cm^{-1}, and 968.75 cm^{-1}, respectively, as illustrated by the dotted lines in Fig. 4. The modes (1, 0), (1, 1), and (2, 0) for the array of lattice parameter 3.0 μm appear at 959.38 cm^{-1}, 1350.00 cm^{-1}, and 1916.41 cm^{-1}, respectively. The

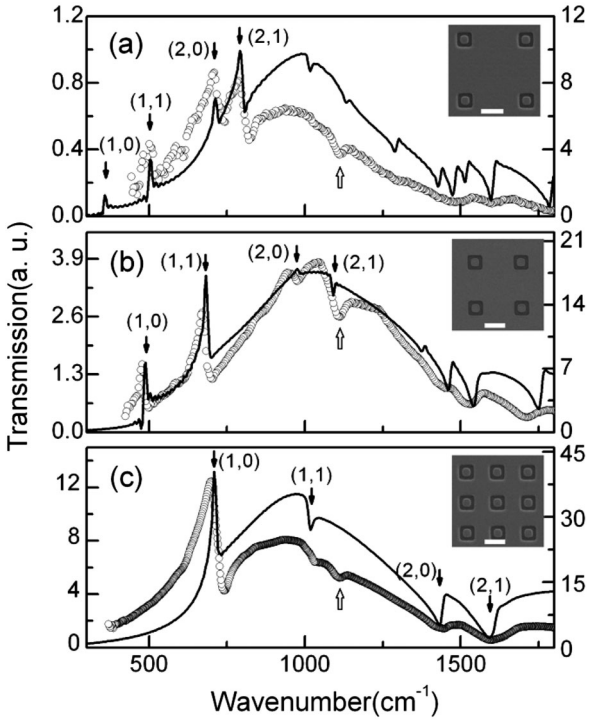

FIG. 3. The transmission spectra of ring-shaped aperture arrays with different lattice parameters: (a) 8.0 μm, (b) 6.0 μm, (c) 4.0 μm. The bar in the inset represents 3.0 μm. The solid lines are the calculated spectra and the open circles are the experimental data.

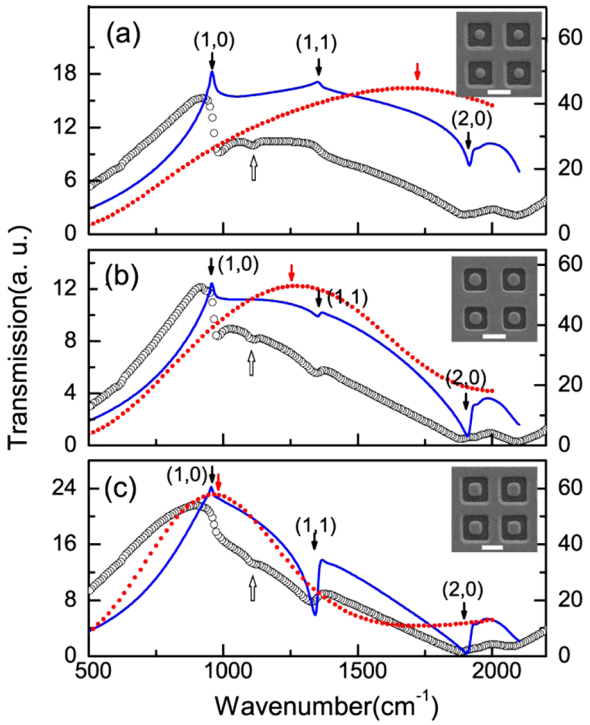

FIG. 4 (color online). The transmission spectra of ring-shaped aperture arrays with different central patch sizes: (a) 0.6 μm, (b) 0.8 μm, (c) 1.0 μm. The lattice parameter is kept at 3.0 μm and the outer rim of the aperture is fixed at 2.0 μm for all cases. The resonant feature of each individual aperture is illustrated by the dotted line, with the gray arrow indicating the resonant frequency. The solid lines are the calculated spectra, and open circles are the experimental data. The bar in the inset represents 2.0 μm.

mode (1, 0) is below ν_0 for all cases. So a peak always emerges for the (1, 0) mode in these scenarios. When the patch size is 0.6 μm, the frequency of resonance mode (1, 1) is below ν_0 ($\nu_0 = 1684.57$ cm^{-1}); hence, the transmission is enhanced. When the patch size is increased to 0.8 μm and 1.0 μm, the frequency of the (1, 1) mode becomes higher than ν_0; hence, a dip appears for the (1, 1) mode in these two scenarios. For mode (2, 0), its frequency is always higher than ν_0 for all cases; therefore, only dips are observed for the (2, 0) mode.

It is noteworthy that in Figs. 3 and 4 the amplitude of the interference peaks and dips is less pronounced than the bump corresponding to LSM. Although adjusting the parameters of ASWA does induce an evident interchange of peaks and dips, in the midinfrared region, the change of intensity is unfortunately limited. However, this effect will be enhanced when the wavelength is shortened.

To summarize, we demonstrate that the interference of the propagating surface Bloch mode and localized surface mode affects the transmission through ASWA; hence, the extrema in the transmission spectrum can be effectively tuned. We suggest that it provides additional clues to understand the nature of extraordinary transmission through subwavelength-aperture arrays.

Support from the MOST of China (No. 2004CB619005 and No. 2006CB921804) and the NSFC (No. 10625417 and No. 10021001) is gratefully acknowledged. The authors also thank Professor Mari-Anne Rosario and Dr. Rupert Oulton for critical reading of the manuscript.

*To whom correspondence should be addressed.
muwang@nju.edu.cn; rwpeng@nju.edu.cn

[1] T. W. Ebbesen, H. J. Lezec, H. F. Ghaemi, T. Thio, and P. A. Wolff, Nature (London) **391**, 667 (1998).
[2] E. Altewischer, M. P. van Exter, and J. P. Woerdman, Nature (London) **418**, 304 (2002).
[3] W. L. Barnes, A. Dereux, and T. W. Ebbesen, Nature (London) **424**, 824 (2003).
[4] N. Ocelic and R. Hillenbrand, Nature Mater. **3**, 606 (2004).
[5] J. B. Pendry, L. Martin-Moreno, and F. J. Garcia-Vidal, Science **305**, 847 (2004).
[6] J. Bravo-Abad *et al.*, Nature Phys. **2**, 120 (2006).
[7] Y. J. Bao *et al.*, Appl. Phys. Lett. **92**, 151902 (2008).
[8] Z. H. Tang *et al.*, Phys. Rev. B **76**, 195405 (2007).
[9] T. Matsui, A. Agrawal, A. Nahata, and Z. V. Vardeny, Nature (London) **446**, 517 (2007).
[10] G. Gay *et al.*, Nature Phys. **2**, 262 (2006).
[11] H. Liu and P. Lalanne, Nature (London) **452**, 728 (2008).
[12] C. Genet and T. W. Ebbesen, Nature (London) **445**, 39 (2007).
[13] L. Martin-Moreno *et al.*, Phys. Rev. Lett. **86**, 1114 (2001).
[14] W. C. Liu and D. P. Tsai, Phys. Rev. B **65**, 155423 (2002).
[15] A. Degiron, H. J. Lezec, N. Yamamoto, and T. W. Ebbesen, Opt. Commun. **239**, 61 (2004).
[16] E. Popov *et al.*, Appl. Opt. **44**, 2332 (2005).
[17] K. L. van der Molen *et al.*, Phys. Rev. B **72**, 045421 (2005).
[18] Z. Ruan and M. Qiu, Phys. Rev. Lett. **96**, 233901 (2006).
[19] H. F. Schouten *et al.*, Phys. Rev. Lett. **94**, 053901 (2005).
[20] G. Gay, O. Alloschery, B. V. de Lesegno, J. Weiner, and H. J. Lezec, Phys. Rev. Lett. **96**, 213901 (2006).
[21] P. Lalanne and J. P. Hugonin, Nature Phys. **2**, 551 (2006).
[22] S. I. Bozhevolnyi, V. S. Volkov, E. Devaux, J. Y. Laluet, and T. W. Ebbesen, Nature (London) **440**, 508 (2006).
[23] F. Lopez-Tejeira *et al.*, Nature Phys. **3**, 324 (2007).
[24] R. Zia and M. L. Brongersma, Nature Nanotech. **2**, 426 (2007).
[25] See EPAPS Document No. E-PRLTAO-101-005835 for supplemental material. For more information on EPAPS, see http://www.aip.org/pubservs/epaps.html.
[26] D. M Sullivan, *Electromagnetic Simulation Using the FDTD Method* (IEEE Press, New Jersey, 2000).
[27] B. A. Munk, *Frequency Selective Surface* (John Wiley & Sons, New York, 2000).
[28] H. J. Pain, *The Physics of Vibrations and Waves* (John Wiley & Sons, New York, 2005).
[29] V. Raghunathan, R. Shori, O. M. Stafsudd, and B. Jalali, Phys. Status Solidi A **203**, R38 (2006).